Engineering Optimization
Vol. 00, No. 00, June 2010, 1–27

RESEARCH ARTICLE

Multi-Step Optimization Strategy for Fuel-Optimal Orbital Transfer of Low-Thrust Spacecraft

M. Rasotto[a], R. Armellin [b*], and P. Di Lizia[c]

[a] *Junior Engineer, Dinamica Srl, Milano, Italy*
[b] *Aeronautics, Astronautics and Computational Engineering Academic Unit, University of Southampton, Southampton, UK*
[c] *Department of Aerospace Science and Technology, Politecnico di Milano, Milano, Italy*

(*v3.7 released September 2008*)

An effective method for the design of fuel-optimal transfers in two- and three-body dynamics is presented. The optimal control problem is formulated using calculus of variation and primer vector theory. This leads to a multi-point boundary value problem (MPBVP), characterized by complex inner constraints and a discontinuous thrust profile. The first issue is addressed by embedding the MPBVP in a parametric optimization problem, thus allowing a simplification of the set of transversality constraints. The second problem is solved by representing the discontinuous control function by a smooth function depending on a continuation parameter. The resulting trajectory optimization method can deal with different intermediate conditions, and no a priori knowledge of the control structure is required. Test cases in both the two- and three-body dynamics show the capability of the method in solving complex trajectory design problems.

Keywords: Optimal control theory; Trajectory optimization; Low-thrust transfers; Hybrid optimization methods

1. Introduction

Low-thrust propulsion is considered as the best option for many future interplanetary transfers. Its higher specific impulse, compared to the traditional chemical propulsion, generally allows the payload-to-spacecraft mass ratio to be improved. In particular, low-thrust propulsion is an ideal option for missions to small objects (comets and aster-

*Corresponding author. Email: roberto.armellin@soton.ac.uk

ISSN: 0305-215X print/ISSN 1029-0273 online

DOI: 10.1080/0305215YYxxxxxxxx
http://www.informaworld.com

oids) for which no large and instantaneous deceleration is required at target arrival (Russel et al. 2005, Kuninaka et al. 2005, Raymanet al. 2000).

On the other hand, transfer times are generally longer with respect to impulsive trajectories, so that low-thrust solutions are best suited to unmanned missions. The design of low-thrust transfers is also much more complex than that of impulsive ones, since the propulsion system needs to be active for large portions of the transfer; therefore the control variables must be modeled as continuous functions and an optimal control problem must be formulated and solved adequately. The optimization of this kind of trajectories is rather difficult and it still represents a challenge for mission designers, despite the numerous techniques developed over the years.

The methods developed for the solution of the optimal control problem can be categorized as direct and indirect methods. In the direct methods the control is parametrized and the dynamics are translated into a set of nonlinear constraints using discretization techniques. The optimal control problem is reduced to a large parametric optimization problem solved with nonlinear programming tools. The implementation of direct methods is straightforward even when many intermediate constraints are considered. A variety of different direct approaches exist, based on the method used to discretize the problem. This includes direct transcription/collocation (Hargraves and Paris 1987, Enright and Conway 1992, Betts 1998, Herman and Conway 1998) and differential inclusion (Conway and Larson 1998, Hargens and Coverstone 2002). The two main drawbacks of direct methods are the high dimensionality of the problem and the convergence to suboptimal solutions, when the parametrization of the control does not fully cover the optimal control space.

Indirect methods find optimum solutions more accurately and produce a numerical problem with lower dimension (Jain and Tsiotras 2008). These methods formulate the optimal control problem as a boundary value problem (BVP) by means of the calculus of variations and the Pontryagin's maximum principle (PMP) (Pontryagin et al. 1962, Lawden 1963, Bryson and Ho 1975, Sauer 1973, Marec 1979). The main drawback of indirect methods is that the convergence domain is small and heavily depends on the quality of the initial guesses, especially for costate variables. Moreover, the fuel-optimal solution has in general a "bang-bang" control profile with switching structure not known a priori. This further increments the difficulty in solving the BVP, e.g. because the integrated functions are not continuous and the Jacobian of the problem is singular.

Different approaches have been proposed to mitigate the difficulties associated with the use of indirect methods. This includes assigning the switching structure a priori(La Mantia and Casalino 2006), using the model of fuel consumption rate proportional to the quadratic of thrust magnitude (Vadali 2001), and reducing the dimension of the problem considered (Mengali and Quarta 2007). Bertrand and Epenoy (2002) also proposed the use of smoothing techniques with a continuation method to limit numerical issues and solve the interplanetary transfer problem accurately.

In this paper, the implementation of an effective method for the optimization of complex low-thrust transfers using an indirect optimization approach is presented. Specifically, in order to simplify the formulation of multi-point boundary value problem (MPBVP) some of the design parameters (such as the departure, arrival, and encounter dates) are considered fixed in the optimal control problem formulation. The optimization of these variables is restored by embedding the MPBVP in a parametric optimization problem, where these parameters are included in the optimization vector. The same approach is adopted to avoid dealing with inequality constraints when gravity assists are included in the transfer: fixed pericenter radii are considered and the optimization of their values

is achieved by including them in the optimization vector of the parametric optimization problem. The proposed approach falls in the category of the so-called hybrid methods (Kluver and Pierson 1995, Gao and Kluver 2004, Russel 2007, Ozimek and Howell 2010), but here the problem simplification is obtained by decomposition of multi-phase trajectories into a sequence of state-to-state transfers.

A continuation approach is proposed to facilitate the convergence to the optimal solution. Thus, a sequence of smooth problems is solved until the last step, when the original fuel-optimal problem is addressed.

Two additional practical techniques are adopted for the optimization of transfers in the three-body dynamics: the adjoint control transformation (ACT) developed by Ranieri and Ocampo (2005) and an off-line global optimizer.

The paper is organized as follows. Section 2 illustrates the equations of motion in the two-body model, along with their respective boundary conditions. The developed approach is described in Section 3, whereas the results are presented in Section 4. In Section 5 the method is customized for its use in the circular restricted three-body problem (CRTBP), and additional results are reported. Final remarks are made in Section 6.

2. Problem Statement

Sections 2–4 are devoted to formulate and solve interplanetary transfers in the two-body dynamics using patched conics approximation. Within this formulation, the transfer is split into a sequence of controlled two-body problems patched together by intermediate events (rendezvous, flybys, and gravity assists). In particular, gravity assists are assumed to occur instantaneously.

2.1. *Equations of Motion*

The general equations of motion of a controlled spacecraft are

$$\begin{cases} \dot{\boldsymbol{r}} &= \boldsymbol{v} \\ \dot{\boldsymbol{v}} &= \boldsymbol{g}(\boldsymbol{r},\boldsymbol{v}) + \dfrac{T_{max}u}{m}\boldsymbol{\alpha} \\ \dot{m} &= -\dfrac{T_{max}u}{I_{sp}g_0} \end{cases} \tag{1}$$

where $\boldsymbol{r}$ and $\boldsymbol{v}$ are the position and velocity vectors, m is the spacecraft mass, T_{max} is the maximum thrust available, I_{sp} is the thruster specific impulse and g_0 is the standard gravitational acceleration. For what concerns the control variables, $u \in [0,1]$ is the thrust ratio and $\boldsymbol{\alpha}$ its direction, so that the control vector can be expressed as $\boldsymbol{u} = u\boldsymbol{\alpha}$. In the two-body approximation, the dynamics reduce to

$$\boldsymbol{g}(\boldsymbol{r}) = -\frac{\mu}{r^3}\boldsymbol{r} \tag{2}$$

in which μ is gravitational parameter of the main attractor. In addition, $r \triangleq \|\boldsymbol{r}\|$. The same notation holds throughout the paper: regular typeface font is used to indicated the norm of the associated vector quantities, which are reported in bold.

2.2. *Boundary Conditions*

The trajectory starts at time t_0 when the spacecraft leaves the sphere of influence (Kaplan 1976) of the departure body, e.g. the Earth. The generic initial boundary conditions can be formulated as

$$\boldsymbol{\Psi}^0 \triangleq \begin{bmatrix} \boldsymbol{r}(t_0) - \boldsymbol{r}_b(t_0) \\ \boldsymbol{v}(t_0) - \boldsymbol{v}_b(t_0) - v_\infty^0 \boldsymbol{u}_{\alpha,\delta}^0 \\ m(t_0) - m_0 \end{bmatrix} = 0 \tag{3}$$

where $\boldsymbol{r}_b$ and $\boldsymbol{v}_b$ are the position and velocity vectors of the celestial body. The first two constraints simply state that the initial position and velocity of the spacecraft must coincide with those of the departing body. In particular, the second condition uses spherical coordinates, thus introducing two angles the azimuth α and declination δ, and a unit vector $\boldsymbol{u}_{\alpha,\delta}^0$, which depends on them. The value v_∞^0 represents the speed at the sphere of influence of the departure body. The last equation constrains the mass at the initial time to be equal to the launch mass.

At the final time (labelled with subscript f), the boundary conditions are

$$\boldsymbol{\Psi}^f \triangleq \begin{bmatrix} \boldsymbol{r}(t_f) - \boldsymbol{r}_b(t_f) \\ \boldsymbol{v}(t_f) - \boldsymbol{v}_b(t_f) - v_\infty^f \boldsymbol{u}_{\alpha,\delta}^f \end{bmatrix} = 0 \tag{4}$$

which can express a rendezvous with ($v_\infty^f = 0$) or a flyby of the arrival celestial body ($v_\infty^f \neq 0$). There is no constraint on the final mass, since it is usually the performance index to be maximized.

2.3. *Intermediate Constraints*

The problem with only initial and arrival constraints defines the so-called planet-to-planet transfer. More complex transfers, with intermediate gravity assists, flybys or rendezvous, are frequently encountered in the design of interplanetary missions and are therefore included in the developed tool.

2.3.1. *Flyby*

The spacecraft positions just before and after a flyby are both required to be equal to the encountered body position, and the spacecraft velocity just before and after the flyby to be continuous. The encountered body (an asteroid, a comet, or a small planet) is assumed to have negligible mass compared to the primary and thus does not produce any effect on the spacecraft trajectory. Also the spacecraft mass is assumed to be continuous throughout the flyby, because no maneuvers are considered.

The complete set of constraints is

$$\boldsymbol{\Psi}_{fb}^i \triangleq \begin{bmatrix} \boldsymbol{r}(t_i^-) - \boldsymbol{r}_b(t_i) \\ \boldsymbol{r}(t_i^+) - \boldsymbol{r}(t_i^-) \\ \boldsymbol{v}(t_i^+) - \boldsymbol{v}(t_i^-) \\ m(t_i^+) - m(t_i^-) \end{bmatrix} = 0 \tag{5}$$

where the superscripts $+$ and $-$ denote the state immediately before and after the flyby at time t_i, and properties of the encountered body are labeled with b.

2.3.2. *Rendezvous*

In a rendezvous, the trajectory of the spacecraft and the celestial body become identical at time t_i. Thus, differently from a flyby, also the velocity of the spacecraft is constrained to match that of the target object. The mass is required to be continuous throughout the maneuver.

The complete set of constraints is given by

$$\boldsymbol{\Psi}^i_{rdv} \triangleq \begin{bmatrix} \boldsymbol{r}(t_i^-) - \boldsymbol{r}_b(t_i) \\ \boldsymbol{r}(t_i^+) - \boldsymbol{r}(t_i^-) \\ \boldsymbol{v}(t_i^-) - \boldsymbol{v}_b(t_i) \\ \boldsymbol{v}(t_i^+) - \boldsymbol{v}(t_i^-) \\ m(t_i^+) - m(t_i^-) \end{bmatrix} = 0 \tag{6}$$

2.3.3. *Gravity Assist*

As for a flyby, the spacecraft positions just before and after the gravity assist must be continuous and equal to the celestial body position. The spacecraft hyperbolic excess velocity, denoted by $\boldsymbol{v}_\infty$, must be unaltered in magnitude. Thus, the set of equality constraints is

$$\boldsymbol{\Psi}^i_{ga} \triangleq \begin{bmatrix} \boldsymbol{r}(t_i^-) - \boldsymbol{r}_b(t_i) \\ \boldsymbol{r}(t_i^+) - \boldsymbol{r}(t_i^-) \\ v_\infty(t_i^+) - v_\infty(t_i^-) \\ m(t_i^+) - m(t_i^-) \end{bmatrix} = 0 \tag{7}$$

Furthermore, the following constraint must be satisfied

$$r_{p_{min}} - r_p \leq 0 \tag{8}$$

in which r_p is the pericenter radius of the hyperbolic planetocentric trajectory and $r_{p_{min}}$ is the lowest admissible value. The value of r_p is computed by applying classical orbital mechanics formulae (Fortescue 2011).

2.3.4. *Free Point*

A free point is used to split the trajectory into multiple segments and this is particularly useful when solving long duration, multiple revolution, or very sensitive trajectories. The constraints associated to a free point are

$$\boldsymbol{\Psi}^i_{fp} \triangleq \begin{bmatrix} \boldsymbol{r}(t_i^+) - \boldsymbol{r}(t_i^-) \\ \boldsymbol{v}(t_i^+) - \boldsymbol{v}(t_i^-) \\ m(t_i^+) - m(t_i^-) \end{bmatrix} = 0 \tag{9}$$

2.4. *Optimal Control Problem Formulation*

The goal of the optimal control problem (OCP) is to minimise the mass of the fuel needed to accomplish the transfer

$$\mathcal{J} = \frac{T_{max}}{I_{sp} g_0} \int_{t_0}^{t_f} u dt \tag{10}$$

Note that a fixed-time formulation is considered. The OCP can be transformed into MPBVP by the use of the calculus of variations and the PMP. Introducing the costate vector $\boldsymbol{\lambda} = \left[\boldsymbol{\lambda}_r; \boldsymbol{\lambda}_v; \lambda_m\right]$, the Hamiltonian is given by

$$\mathcal{H} = \boldsymbol{\lambda}_{\boldsymbol{r}}^T \boldsymbol{v} + \boldsymbol{\lambda}_{\boldsymbol{v}}^T \left(-\frac{\mu}{r^3}\boldsymbol{r} + \frac{T_{max}u}{m}\boldsymbol{\alpha} \right) - \lambda_m \frac{T_{max}}{I_{sp}g_0}u + \frac{T_{max}}{I_{sp}g_0}u \tag{11}$$

By minimizing the Hamiltonian with respect to the control variables u and $\boldsymbol{\alpha}$, the Lawden's primer vector control law is obtained, as given in Eq. (12)

$$\boldsymbol{\alpha} = -\frac{\boldsymbol{\lambda}_v}{\lambda_v}, \qquad u = \begin{cases} 0 & \text{if} \quad \rho > 0 \\ 1 & \text{if} \quad \rho < 0 \\ 0 \leq u \leq 1 & \text{if} \quad \rho = 0 \end{cases} \tag{12}$$

where the switching function ρ is defined as

$$\rho = 1 - \frac{I_{sp}g_0}{m}\lambda_v - \lambda_m \tag{13}$$

Since ρ takes the value of zero only at finite isolated points, u is either zero or one on any interval. Thus, the thrust is either zero or maximum along the optimal solution, leading to a "bang-bang" control profile. According to the PMP, the costates equations are given by

$$\dot{\boldsymbol{\lambda}} = -\mathcal{H}_{\boldsymbol{x}} = \begin{cases} \dot{\boldsymbol{\lambda}}_r = \dfrac{\mu}{r^3}\boldsymbol{\lambda}_v - \dfrac{3\mu \boldsymbol{r}\cdot\boldsymbol{\lambda}_v}{r^5}\boldsymbol{r} \\ \dot{\boldsymbol{\lambda}}_v = -\boldsymbol{\lambda}_r \\ \dot{\lambda}_m = -\dfrac{T_{max}u}{m^2}\lambda_v \end{cases} \tag{14}$$

in which the subscript $\boldsymbol{x}$ refers to the partial derivative with respect to the state vector $\boldsymbol{x} = [\boldsymbol{r}; \boldsymbol{v}; m]$.

Finally, the transversality conditions can be written as

$$\boldsymbol{\lambda}^T(t_0) = \boldsymbol{\nu}_0^T \boldsymbol{\Psi}_{\boldsymbol{x}}^0 \tag{15}$$

$$\boldsymbol{\lambda}^T(t_i^-) = \boldsymbol{\pi}^T \boldsymbol{\Psi}_{\boldsymbol{x}}^i \tag{16}$$

$$\boldsymbol{\lambda}^T(t_i^+) = -\boldsymbol{\pi}^T \boldsymbol{\Psi}_{\boldsymbol{x}}^i \tag{17}$$

$$\boldsymbol{\lambda}^T(t_f) = \boldsymbol{\nu}_f^T \boldsymbol{\Psi}_{\boldsymbol{x}}^f \tag{18}$$

where $\boldsymbol{\nu}_0$, $\boldsymbol{\nu}_f$ and $\boldsymbol{\pi}$ are the adjoint multipliers associated with initial, final and interior-point constraints. The application of these relations leads to different conditions, depending on the intermediate maneuver considered, and also defines the complete set of variables of the MPBVP.

3. Numerical Approach to the Optimal Control Problem

The numerical techniques developed for the solution of the OCP and the corresponding MPBVP are presented in this section. The following sections cover:

(1) Embedding of the MPBVP in a parametric optimization problem;
(2) Solution of an energy-OCP to obtain first guesses for the Lagrangian multipliers;
(3) A $\mathcal{C}^\infty$ approximation of the discontinuous optimal control law and solution of a sequence of fuel-OCPs before switching to the exact discontinuous one.

3.1. *Optimal Control Problem Discretization*

In this work the MPBVP is solved with an indirect multiple shooting technique (Bulirsch and Stoer 2002). Let the overall trajectory be decomposed into N segments, each of them starting at a node i. The first node of a segment can be either the trajectory departure or an intermediate event (e.g. a gravity assist), and the second node can be either the arrival or a successive event (e.g. a second gravity assist). Adopting the notation of Olympio (2011), each node includes a set of decision variables, a set of initial conditions $\boldsymbol{C}^i$ and a set of constraints $\boldsymbol{\Psi}^i$. The conditions and constraints depend on the type of the event and are summarised in Table 1. Differently from Olympio (2011), $\boldsymbol{\xi^i}$ refer to the decision variables associated to the MPBVP whereas $\boldsymbol{\chi^i}$ are the variables of the parametric optimization problem introduced to simplify the OCP transversality conditions. These variables are considered fixed in the solution of the OCP.

From Table 1 it can be seen that, for intermediate events, the $\boldsymbol{\chi^i}$ vector includes the time of the events t_i. For a gravity assist also the pericenter radius r_{p_i} is included. In this case, setting appropriate bounds on $\chi^i_{r_p}$ allows the solution to automatically satisfy the constraint on the minimum pericenter radius and avoids dealing with inequality constraints in the formulation of the OCP.

For the first node, the initial conditions are

$$\boldsymbol{C}^0 \triangleq \begin{bmatrix} \boldsymbol{r}(t_0) = \boldsymbol{r}_b(t_0) \\ \boldsymbol{v}(t_0) = \boldsymbol{v}_b(t_0) + \chi^0_{v_\infty} \boldsymbol{\chi}^0_{\boldsymbol{u}_{\alpha,\delta}} \\ m(t_0) = m_0 \\ \boldsymbol{\lambda_r}(t_0) = \boldsymbol{\xi}^0_{\boldsymbol{\lambda_r}} \\ \boldsymbol{\lambda_v}(t_0) = \boldsymbol{\xi}^0_{\boldsymbol{\lambda_v}} \\ \lambda_m(t_0) = \xi^0_{\lambda_m} \end{bmatrix} \tag{19}$$

In this case, $\boldsymbol{\chi}^0$ also includes the relative velocity at the sphere of influence of the departing body, which means an OCP with fixed initial state is considered. When the initial speed at the sphere of influence is assigned, the constraints on the velocity reduce to

$$\boldsymbol{v}(t_0) = \boldsymbol{v}_b(t_0) + v^0_\infty \boldsymbol{\chi}^0_{\boldsymbol{u}_{\alpha,\delta}} \tag{20}$$

in which v^0_∞ is a user-defined parameter. In the general case, the decision variables for the first node are then

$$\begin{aligned} \boldsymbol{\xi^0} &= [\boldsymbol{\xi}^0_{\boldsymbol{\lambda_r}}; \boldsymbol{\xi}^0_{\boldsymbol{\lambda_v}}; \xi^0_{\lambda_m}] \\ \boldsymbol{\chi^0} &= [\chi_{t_0}; \chi^0_{v_\infty}; \boldsymbol{\chi}^0_{\boldsymbol{u}_{\alpha,\delta}}] \end{aligned} \tag{21}$$

Table 1. Intermediate decision variables, constraints, and conditions

	Decision variables $\boldsymbol{\xi}^i$, $\boldsymbol{\chi}^i$	Implemented constraints $\boldsymbol{\Psi}^i$	Implemented conditions $\boldsymbol{C}^i$
Flyby	$\boldsymbol{\xi}^i_{\boldsymbol{v}}$, ξ^i_m $\boldsymbol{\xi}^i_{\boldsymbol{\lambda}_r}$, $\boldsymbol{\xi}^i_{\boldsymbol{\lambda}_v}$, $\xi^i_{\lambda_m}$ χ^i_t	$\boldsymbol{r}(t_i^-) - \boldsymbol{r}_b(t_i) = 0$ $\boldsymbol{v}(t_i^-) - \boldsymbol{\xi}^i_{\boldsymbol{v}} = 0$ $m(t_i^-) - \xi^i_m = 0$ $\boldsymbol{\lambda}_{\boldsymbol{v}}(t_i^-) - \boldsymbol{\xi}^i_{\boldsymbol{\lambda}_v} = 0$ $\lambda_m(t_i^-) - \xi^i_{\lambda_m} = 0$	$\boldsymbol{r}(t_i^+) = \boldsymbol{r}_b(t_i)$ $\boldsymbol{v}(t_i^+) = \boldsymbol{\xi}^i_{\boldsymbol{v}}$ $m(t_i^+) = \xi^i_m$ $\boldsymbol{\lambda}_{\boldsymbol{r}}(t_i^+) = \boldsymbol{\xi}^i_{\boldsymbol{\lambda}_r}$ $\boldsymbol{\lambda}_{\boldsymbol{v}}(t_i^+) = \boldsymbol{\xi}^i_{\boldsymbol{\lambda}_v}$ $\lambda_m(t_i^+) = \xi^i_{\lambda_m}$
Rendezvous	ξ^i_m $\boldsymbol{\xi}^i_{\boldsymbol{\lambda}_r}$, $\boldsymbol{\xi}^i_{\boldsymbol{\lambda}_v}$, $\xi^i_{\lambda_m}$ χ^i_t	$\boldsymbol{r}(t_i^-) - \boldsymbol{r}_b(t_i) = 0$ $\boldsymbol{v}(t_i^-) - \boldsymbol{v}_b(t_i) = 0$ $m(t_i^-) - \xi^i_m = 0$ $\lambda_m(t_i^-) - \xi^i_{\lambda_m} = 0$	$\boldsymbol{r}(t_i^+) = \boldsymbol{r}_b(t_i)$ $\boldsymbol{v}(t_i^+) = \boldsymbol{v}_b(t_i)$ $m(t_i^+) = \xi^i_m$ $\boldsymbol{\lambda}_{\boldsymbol{r}}(t_i^+) = \boldsymbol{\xi}^i_{\boldsymbol{\lambda}_r}$ $\boldsymbol{\lambda}_{\boldsymbol{v}}(t_i^+) = \boldsymbol{\xi}^i_{\boldsymbol{\lambda}_v}$ $\lambda_m(t_i^+) = \xi^i_{\lambda_m}$
Gravity Assist	$\boldsymbol{\xi}^i_{\boldsymbol{v}}$, ξ^i_m $\boldsymbol{\xi}^i_{\boldsymbol{\lambda}_r}$, $\boldsymbol{\xi}^i_{\boldsymbol{\lambda}_v}$, $\xi^i_{\lambda_m}$ ξ^i_ν $\chi^i_{r_p}$, χ^i_t	$\boldsymbol{r}(t_i^-) - \boldsymbol{r}_b(t_i) = 0$ $v_\infty^- - v_\infty^+ = 0$ $m(t_i^-) - \xi^i_m = 0$ $\boldsymbol{\lambda}_{\boldsymbol{v}}(t_i^-) - 2\xi^i_\nu \boldsymbol{v}_\infty^- = 0$ $2\xi^i_\nu \boldsymbol{v}_\infty^+ - \boldsymbol{\xi}^i_{\boldsymbol{\lambda}_v} = 0$ $\lambda_m(t_i^-) - \xi^i_{\lambda_m} = 0$ $r^i_{ph} - \chi^i_{r_p} = 0$	$\boldsymbol{r}(t_i^+) = \boldsymbol{r}_b(t_i)$ $\boldsymbol{v}(t_i^+) = \boldsymbol{\xi}^i_{\boldsymbol{v}}$ $m(t_i^+) = \xi^i_m$ $\boldsymbol{\lambda}_{\boldsymbol{r}}(t_i^+) = \boldsymbol{\xi}^i_{\boldsymbol{\lambda}_r}$ $\boldsymbol{\lambda}_{\boldsymbol{v}}(t_i^+) = \boldsymbol{\xi}^i_{\boldsymbol{\lambda}_v}$ $\lambda_m(t_i^+) = \xi^i_{\lambda_m}$
Free Point	$\boldsymbol{\xi}^i_{\boldsymbol{r}}$, $\boldsymbol{\xi}^i_{\boldsymbol{v}}$, ξ^i_m $\boldsymbol{\xi}^i_{\boldsymbol{\lambda}_r}$, $\boldsymbol{\xi}^i_{\boldsymbol{\lambda}_v}$, $\xi^i_{\lambda_m}$ χ^i_t	$\boldsymbol{r}(t_i^-) - \boldsymbol{\xi}^i_{\boldsymbol{r}} = 0$ $\boldsymbol{v}(t_i^-) - \boldsymbol{\xi}^i_{\boldsymbol{v}} = 0$ $m(t_i^-) - \xi^i_m = 0$ $\boldsymbol{\lambda}_{\boldsymbol{r}}(t_i^-) - \boldsymbol{\xi}^i_{\boldsymbol{\lambda}_r} = 0$ $\boldsymbol{\lambda}_{\boldsymbol{v}}(t_i^-) - \boldsymbol{\xi}^i_{\boldsymbol{\lambda}_v} = 0$ $\lambda_m(t_i^-) - \xi^i_{\lambda_m} = 0$	$\boldsymbol{r}(t_i^+) = \boldsymbol{\xi}^i_{\boldsymbol{r}}$ $\boldsymbol{v}(t_i^+) = \boldsymbol{\xi}^i_{\boldsymbol{v}}$ $m(t_i^+) = \xi^i_m$ $\boldsymbol{\lambda}_{\boldsymbol{r}}(t_i^+) = \boldsymbol{\xi}^i_{\boldsymbol{\lambda}_r}$ $\boldsymbol{\lambda}_{\boldsymbol{v}}(t_i^+) = \boldsymbol{\xi}^i_{\boldsymbol{\lambda}_v}$ $\lambda_m(t_i^+) = \xi^i_{\lambda_m}$

For the final node, the corresponding terminal constraints are

$$\boldsymbol{\Psi}^N \triangleq \begin{bmatrix} \boldsymbol{r}(t_f^-) - \boldsymbol{r}_b(t_f) \\ \boldsymbol{v}(t_f^-) - (\boldsymbol{v}_b(t_f) + \chi^N_{v_\infty} \boldsymbol{\chi}^N_{\boldsymbol{u}_{\alpha,\delta}}) \\ m(t_f^-) - \chi^N_m \\ \lambda_m(t_f^-) \end{bmatrix} = 0 \tag{22}$$

If the final condition is a rendezvous then the constraint on the velocity simplifies to

$$\boldsymbol{v}(t_f) - \boldsymbol{v}_b(t_f) = 0 \tag{23}$$

In the general case, the decision vector for the last node is

$$\boldsymbol{\chi}^{\boldsymbol{N}} = [\chi_{t_f}^N; \chi_{v_\infty}^N; \boldsymbol{\chi}_{\boldsymbol{u}_{\alpha,\delta}}^N; \chi_m^N] \tag{24}$$

The assembled vectors of decision variables can be then written as $\boldsymbol{\Xi} = [\boldsymbol{\xi}^0; \ldots; \boldsymbol{\xi}^N]$ and $\boldsymbol{\chi} = [\boldsymbol{\chi}^0; \ldots; \boldsymbol{\chi}^N]$.

For the i–th node, the initial state and costate, extracted from the decision variables, are integrated forward up to the $(i+1)$-th node. At this node there will, in general, be a constraints violation $\boldsymbol{\delta\Psi}_{i+1}$: the OCP is solved when all the constraints violations are driven to zero within a given tolerance.

Due to the introduction of the $\boldsymbol{\chi}$ variables, the number of constraints of the MPBVP is lower then the number of decision variables. Thus, the MPBVP can be embedded in a parametric optimization in which the degrees of freedom given by $\boldsymbol{\chi}$ are used to maximize the final mass of the spacecraft. Note that the final mass itself is part of the $\boldsymbol{\chi}$ as shown in (24), thus the optimization problem is reduced to its Meyer form (Betts 1998).

The parametric optimization problem is solved with a nonlinear quadratic programming method. The required guesses for $\boldsymbol{\chi}$ and the state variables included in $\boldsymbol{\Xi}$ are obtained with a low-fidelity trajectory optimization tool in which low-thrust transfers are approximated by a series of impulsive manoeuvres (Carrara 2007).

3.2. *Energy-Optimal Control Problem*

Nonlinear quadratic programming methods require good initial guesses that lie within the domain of convergence of the optimal solution. This requirement is particularly difficult to satisfy for the costates, whose physical meaning is non-intuitive. In addition, because of the discontinuous nature of the "bang-bang" control law, numerical difficulties in the integration of the Euler-Lagrange differential equations arise. Thus, it is difficult to ensure that the algorithm converges to the optimal solution.

To counteract these issues an easier MPBVP is first considered, with performance index

$$\mathcal{J} = \frac{1}{2}\int_{t_0}^{t_f} \boldsymbol{a}_c^T \boldsymbol{a}_c dt \tag{25}$$

where $\boldsymbol{a}_c$ is the control acceleration. This justifies the name of energy-OCP. Moreover, the control function is continuous and expressed in terms of acceleration

$$\begin{cases} \dot{\boldsymbol{r}} &= \boldsymbol{v} \\ \dot{\boldsymbol{v}} &= -\dfrac{\mu}{r^3}\boldsymbol{r} + \boldsymbol{a}_c \end{cases} \tag{26}$$

The Hamiltonian of this problem changes consequently to

$$\mathcal{H} = \frac{1}{2}\boldsymbol{a}_c^T\boldsymbol{a}_c + \boldsymbol{\lambda}_{\boldsymbol{r}}^T\boldsymbol{v} + \boldsymbol{\lambda}_{\boldsymbol{v}}^T\left(-\frac{\mu}{r^3}\boldsymbol{r} + \boldsymbol{a}_c\right) \tag{27}$$

and its minimization yields the optimal control law

$$\boldsymbol{a}_c = -\boldsymbol{\lambda}_{\boldsymbol{v}} \tag{28}$$

i.e. the acceleration is equal to the velocity costate vector. The costates differential equations are derived

$$\dot{\boldsymbol{\lambda}} = -\mathcal{H}_{\boldsymbol{x}} = \begin{cases} \dot{\boldsymbol{\lambda}}_r = \dfrac{\mu}{r^3}\boldsymbol{\lambda}_v - \dfrac{3\mu \boldsymbol{r}\cdot\boldsymbol{\lambda}_v}{r^5}\boldsymbol{r} \\ \dot{\boldsymbol{\lambda}}_v = -\boldsymbol{\lambda}_r \end{cases} \tag{29}$$

where now the state vector $\boldsymbol{x}$ is given by spacecraft position and velocity only, i.e. $\boldsymbol{x} = [\boldsymbol{r}; \boldsymbol{v}]$.

The main advantage of such a formulation is that the problem is characterized by a continuous control law with significantly larger convergence radius. In the performed tests, the convergence was always achieved using $\boldsymbol{\lambda}_r = \mathbf{0}$ and $\boldsymbol{\lambda}_v = \mathbf{0}$ (i.e., $\boldsymbol{a}_c = \mathbf{0}$) as a first guess solution. This will hold true as long as multi-revolution transfers are not considered, for which a continuation on the time of flight may be necessary.

3.3. *Continuation Method*

The solution of the energy-OCP provides first guess values of the costates for the fuel-OCP, whereas mass costates are generated randomly in the positive interval $[0, 1]$, since it can be shown that $\lambda_m(t_0) \geq 0$ (for details refer to Jiang et al. (2012)). Nevertheless, the solution of the discontinuous problem is still difficult to obtain because of the numerical difficulties associated with the discontinuity of the Euler-Lagrange differential equations. A continuation method is therefore introduced, based on a $\mathcal{C}^\infty$ approximation of the "bang-bang" control law by means of exponential or arc-tangential functions (often used in control theory as analytic approximation of the Heaviside step function):

$$u = \frac{1}{1+\exp\left(2p\rho\right)} \qquad \text{or} \qquad u = \frac{1}{2} + \frac{1}{\pi}\arctan(-p\rho) \tag{30}$$

In both cases, the analytical approximations are controlled by the so-called continuation parameter p, defined in an appropriate partition of the interval $[1, \infty]$. Note that, although derived in a different way, the exponential representation can be already found in Bertrand and Epenoy (2002). Differently from Bertrand and Epenoy (2002), in the present approach the continuation method is applied only to the control representation, while the objective function remains unchanged during the iterations. By heuristically increasing the value of p, the discontinuous behaviour of the control is gradually approximated. The MPBVP is solved using the indirect multiple shooting method presented in Sec. 3.1, and the solution found for p_k is used as first guess for the p_{k+1}. The continuation stops when p reaches a user defined limit p_{max}. Note that during the continuation process the objective function of the parametric optimization problem remains unchanged: $J = -\chi_m^N$.

3.4. *Fuel-Optimal Control Problem*

The final solution obtained from the continuation method is characterized by a $\mathcal{C}^\infty$ control law. Thus, a final optimization is run, in which the discontinuous "bang-bang" control law (12) is considered. Similarly to the previous steps, by using the indirect multiple shooting method presented in Sec. 3.1, the resulting MPBVP is reduced to a parametric optimization problem, solved with a nonlinear quadratic programming approach. A

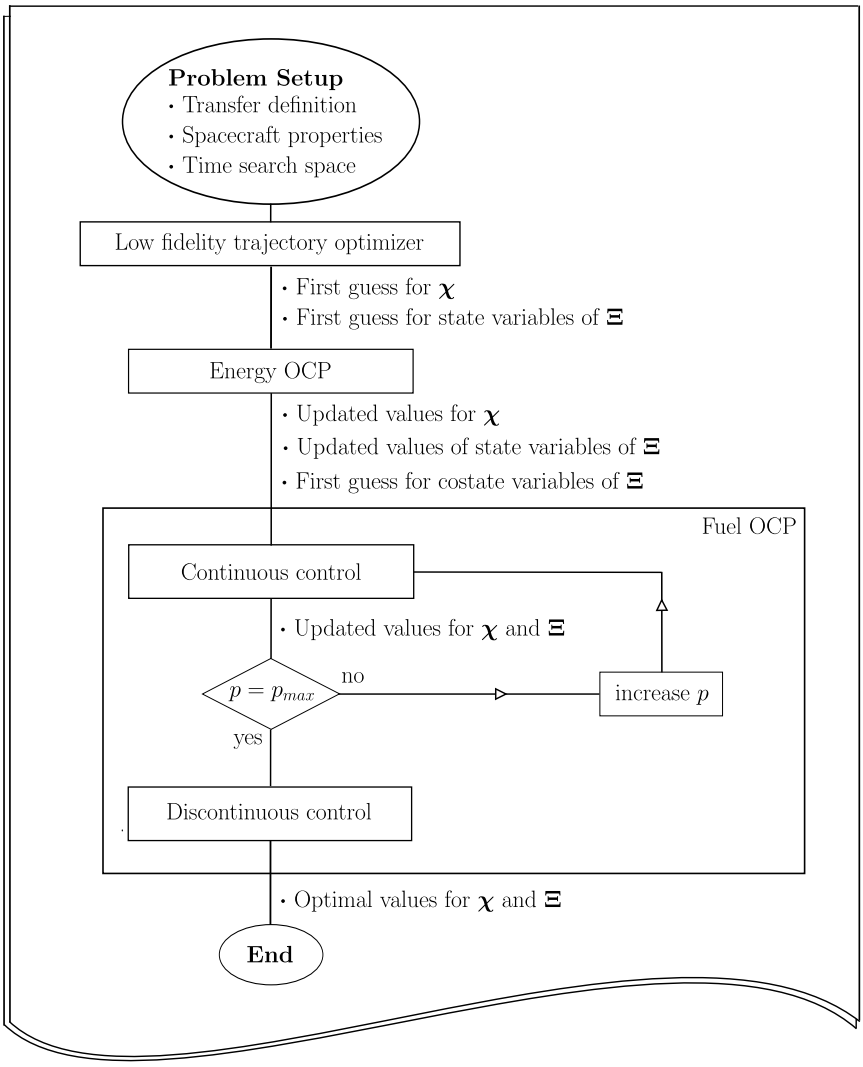

Figure 1. Optimization architecture.

sufficiently high value of p_{max} guarantees the convergence in few iterations.

3.5. *Strategy Workflow*

An overview of the resulting optimization strategy is provided in this section to summarize both its fundamental steps and the algorithm workflow. The strategy is illustrated in the flowchart reported in Figure 1. The process starts with the definition of the transfer to be designed, the spacecraft properties, and the search space for the times of each event. Once the problem is completely defined, a low fidelity trajectory optimizer is used to generate first guesses for the decision vectors $\boldsymbol{\chi}$ and for the state variables in $\boldsymbol{\Xi}$.
The procedure continues by solving the energy-OCP, as explained in Sec. 3.2. This step is basically aimed to easily obtain updated values of the quantities in $\boldsymbol{\chi}$ and $\boldsymbol{\Xi}$, along with first guesses for the costate variables in $\boldsymbol{\Xi}$.
As shown in Figure 1, the last step concerns the resolution of the corresponding fuel

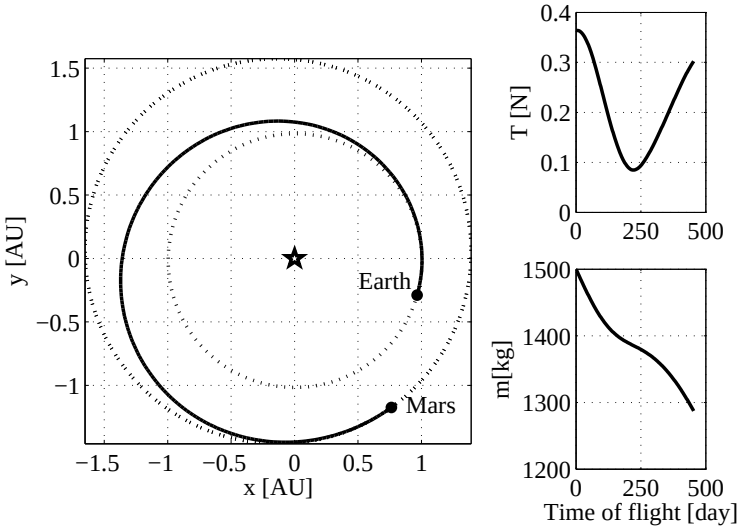

Figure 2. Energy-optimal solution for the Earth–Mars transfer.

optimal problem, which is split in two different phases. In the first phase, the problem is formulated to take advantage of a smoothing approximation of the control, which depends on a smoothing parameter p. Then, the solution is found by continuation: the fuel optimal problem is solved iteratively for increasing values of p until $p = p_{max}$, as described in Section 3.3. Starting from the solution of this first phase, the second one addresses the exact fuel optimal problem by removing the smoothing approximation.

4. Numerical results

4.1. *Earth–Mars Transfer*

The first example is a simple Earth–Mars transfer with an assigned v_∞^0 of 0.2 km/s and final rendezvous conditions. The initial mass of the spacecraft is 1500 kg, and the propulsion system provides a maximum thrust of 0.33 N with a $I_{sp} = 3800$ s. In this simple example the decision vectors are $\boldsymbol{\mathcal{X}} = [\chi_t^0; \boldsymbol{\chi}_{\boldsymbol{u}_{\alpha,\delta}}^0; \chi_t^1; \chi_m^1]$ and $\boldsymbol{\Xi} = [\boldsymbol{\xi}_{\boldsymbol{\lambda}_r}^0; \boldsymbol{\xi}_{\boldsymbol{\lambda}_v}^0; \xi_{\lambda_m}^0]$.

The search space for departure epoch and transfer time are $\chi_t^0 \in [4000, 4300]$ MJD2000 and $\chi_t^1 \in [200, 500]$ days, respectively. The angles χ_α^0, χ_δ^0 for the identification of the direction of $\boldsymbol{v}_\infty^0$ are searched in the intervals $[-\pi, \pi]$ and $[-\pi/2, \pi/2]$. Finally, the final mass χ_m^1 is sought in the interval $[500, 1500]$ kg. The initial Lagrangian multipliers $\boldsymbol{\xi}_{\boldsymbol{\lambda}_r}^0$ and $\boldsymbol{\xi}_{\boldsymbol{\lambda}_v}^0$ belong to the interval $[-\infty, \infty]$, and the search space for the mass multipliers $\xi_{\lambda_m}^0$ is set to $[0, 1]$.

The energy optimal solution obtained is reported in Figure 2. As can be seen, the thrust profile violates the constraint on the maximum thrust at the beginning of the transfer. This behaviour is compatible with the energy-OCP where the control is given in terms of acceleration. In this case the final mass is $m_f = 1287$ kg.

The energy-optimal solution is used as first guess for the fuel-OCP. The exponential approximation of the step function is used with $p = 2^k$ and $k = [1, \ldots, 10]$. From Figure 3

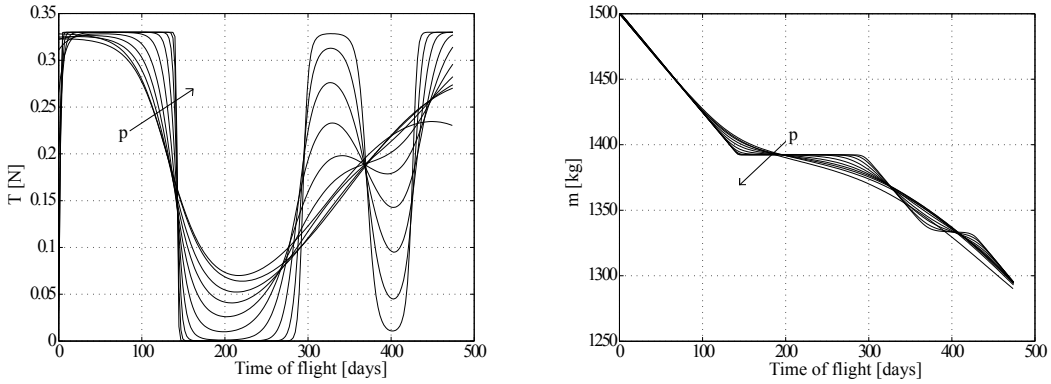

(a) Thrust magnitude profile (b) Mass consumption profile

Figure 3. Smoothing approximation for the Earth–Mars transfer.

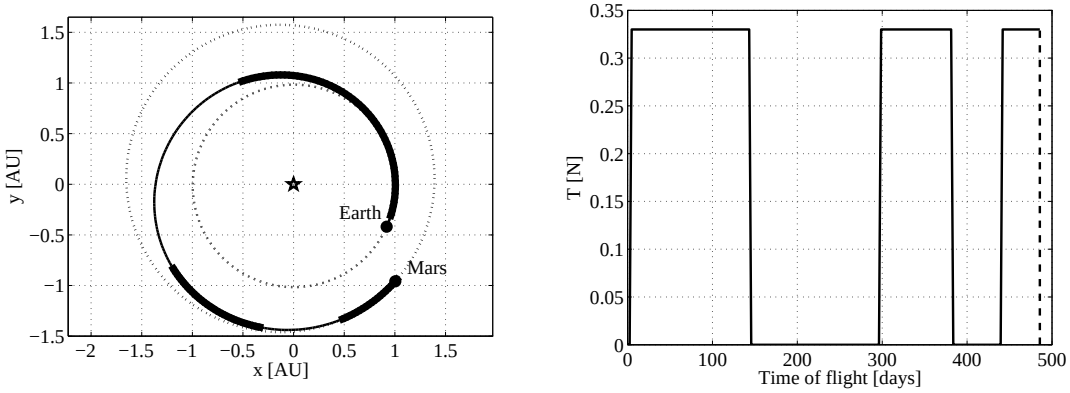

(a) Optimal transfer (b) Thrust profile

Figure 4. Earth-Mars fuel-optimal transfer (thicker lines refer to thrust arcs).

note how the discontinuous behaviour, typical of a "bang-bang" control law, progressively emerges and how this impacts the mass consumption.

The last step is to solve the discontinuous fuel-optimal problem. Figure 4 illustrates the final trajectory and the optimal control amplitude obtained. (In the reminder of the paper thicker lines are used in the trajectory plots to highlight thrust arcs.) By comparing Figure 2 with 4 a slight change in the times can be appreciated: in the energy optimal solution the departure epoch is scheduled for 4265.75 MJD2000, whereas for the fuel optimal solution the spacecraft leaves the Earth on 4260.62 MJD2000. Also the transfer times differ, thus the arrival at Mars occurs on 4719.02 MJD2000 for the energy optimal solution, whereas the planet is reached few days later, on 4735.1 MJD2000, in the fuel optimal one. The final mass is 1295.04, with propellant-to-mass ratio of 13.66%.

Table 2. Earth–Venus transfer times search space and optimal solution

	Departure epoch [MJD2000]	t_{E1} [days]	t_{12} [days]	t_{23} [days]	t_{34} [days]	t_{4V} [days]
Upper Bound	2110	380	190	100	200	300
Lower Bound	2000	280	130	30	110	250
Solution	2105	347.6	160.6	68.4	157.9	257.8

4.2. *Earth–Venus Transfer*

A rendezvous problem with Venus is investigated in this section. This example is presented by Bertrand and Epenoy (2002), and it is also analyzed by Jiang et al. (2012). Both works make use of an indirect approach, although the continuation method adopted is applied to the objective function rather than on the control representation. A spacecraft with the same properties of Sec. 4.1 is considered and a $v_\infty^0 = 0$ is set.

To facilitate the convergence of the optimization method the trajectory is split into 5 different legs by introducing 4 intermediate free points, identified as point 1, point 2, point 3 and point 4. The initial values of these points are taken from the first guess trajectory calculated with by the low-fidelity solver (Carrara 2007). In general there are no bounds on the position and velocity of these points; however bounds on positions are considered to avoid possible overlap between different trajectory legs. Due to the introduction of free intermediate points the total number of variables increases from 12 (as in the Earth–Mars problem) to 70.

The search space for the departure epoch and transfer times together with the optimal solution found are given in Table 2, where the label E is used for the Earth, V for Venus, and the numbers for the intermediate points. The resulting optimal trajectory is presented in Figure 5. The achieved final mass of 1290.3 kg is slightly higher than the one obtained from the solution of the energy-OCP (equal to 1285.4 kg) and comparable to the one reported in the literature, which was 1290 kg (Jiang et al. 2012).

4.3. *Earth–Apophis–Earth Transfer*

A simple single-encounter trajectory, where the spacecraft performs a flyby of the asteroid Apophis and then returns to the Earth, is described in this section. This mission scenario is presented in Olympio (2011).

The spacecraft is assumed to be equipped with a thruster that provides a T_{max} of 0.3 N with $I_{sp} = 2500$ s. The excess velocity after launch is fixed to $v_\infty^0 = 2.5$ km/s, and the initial mass is $m_0 = 1500$ kg. The overall number of unknowns of this problem is 28.

Table 3 defines the search space for the departure epoch and transfer times together with the computed optimal values. The solution is represented in Figure 6 and is characterized by a final mass $m_f = 1432$ kg, which is significantly higher than that reported in the literature of 1137 kg. (It is worth mentioning that in his paper Olympio states "Since relatively little effort has been put into the initial guess, it is likely that better optimal solutions exist"). It is interesting to note that the departure epoch is scheduled only about 46 days before the launch date of the reference solution, whereas the transfer times are comparable. Furthermore, no propulsion is used before Apophis flyby.

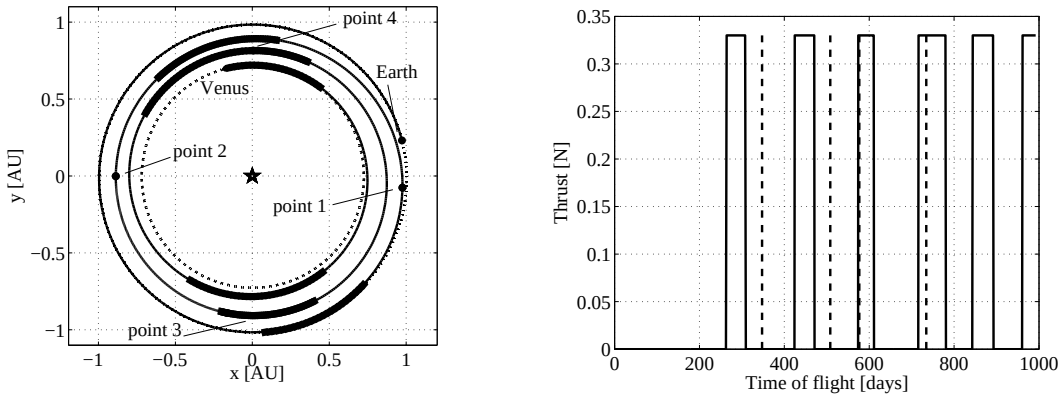

(a) Optimal transfer (thicker lines refer to thrust arcs)

(b) Thrust profile with intermediate points marked with dashes vertical lines

Figure 5. Earth-Venus multiple revolution fuel-optimal transfer.

Table 3. Earth–Apophis–Earth transfer times search space and optimal solution

	Departure epoch [MJD2000]	t_{EA} [days]	t_{AE} [days]
Upper Bound	4518	100	440
Lower Bound	5018	300	300
Solution	4672.19	200.58	438.68

4.4. *A Solution to the Third Global Trajectory Optimization Competition*

This last test case is to show the capability of the method in optimizing trajectories with multiple rendezvous. The problem of the 3^{rd} global trajectory optimization competition (GTOC) edition, organized by Politecnico di Torino in December 2007, is taken as reference. The goal is to design a multiple near-Earth asteroid (NEA) rendezvous with return to the Earth. The spacecraft is to launch from the Earth, with hyperbolic excess velocity v_∞^0 of up to 0.5 km/s and of unconstrained direction. The year of launch must lie in the range 2016 to 2025, inclusive. After launch, the spacecraft must first rendezvous with three different asteroids, taken from a list of 140 asteroids, and then rendezvous with the Earth. The choice of the asteroids is part of the optimisation process. The stay-times at each of the three asteroids must be longer than 60 days. The total time of flight time, measured from launch up to the point of rendezvous with the Earth, must not exceed 10 years. Only gravity assists from the Earth are permitted. The spacecraft has a fixed initial mass of 2000 kg. The propulsion has a constant specific impulse I_{sp} of 3000 s and a maximum thrust level T_{max} of 0.15 N. The performance index to be maximized is a function of the final mass and the stay-time on the asteroids.

The asteroid sequence submitted by the team TAC (The Aerospace Corporation) was used as reference. It exploits the sequence E-88-E-96-49-E, where 88 (1991 VG), 96

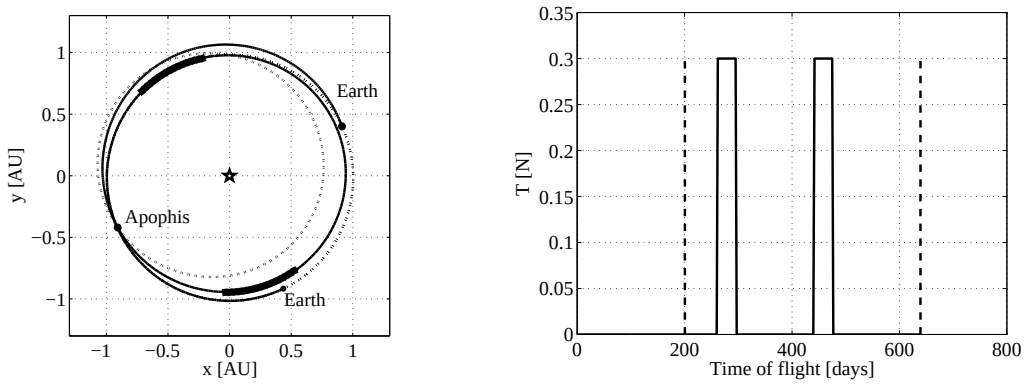

(a) Optimal transfer

(b) Thrust profile with intermediate flyby occurrence marked with a vertical dashed line

Figure 6. Earth-Apophis-Earth fuel-optimal transfer.

Table 4. GTOC search space and optimal solution for departure and transfer times

	Dep. epoch [MJD2000]	t_{E-88} [days]	t_{88-88} [days]	t_{88-E} [days]	t_{E-96} [days]	t_{96-96} [days]	t_{96-49} [days]	t_{49-49} [days]	t_{49-E} [days]
Upper Bound	6800	580	440	800	580	440	580	440	900
Lower Bound	6000	180	60	400	180	60	180	60	500
Solution	6566.1	580	88.1	641.2	440.8	320.0	567.1	294.8	682.1

(2001 GP2), and 49 (2000 SG344) are the asteroids as cataloged in the list provided by the organizers (Casalino et al. 2007) and E is the Earth. The first guess solution for rendezvous and flyby dates is obtained by the low-fidelity trajectory optimization code by Carrara (2007). The bounds for the transfer times listed in Table 4 are such that the optimal solution provided by TAC is included (Casalino et al. 2007). In the proposed formulation the problem is described by 57 unknowns.

The refined trajectory (in which thrust arcs are not highlighted for the sake of clarity) and thrust profile are shown in Fig. 7. In the trajectory plot a square is used to indicate a departure, a circle an arrival, and a triangle a gravity assist. The optimal departure date, transfer, and stay times are given in Table 4. The computed final mass is about 1591 kg, which is 56 kg less than TAC solution. Note that little effort was spent in the generation of a good first guess solution as the goal of the test case was mainly to show the ability of the method to deal with multiple rendezvous missions.

5. Optimal Control Problem in Three-Body Dynamics

In many cases, to support new mission concepts, the motion of the spacecraft needs to be studied in a more general fashion that accounts, for example, the gravitational field

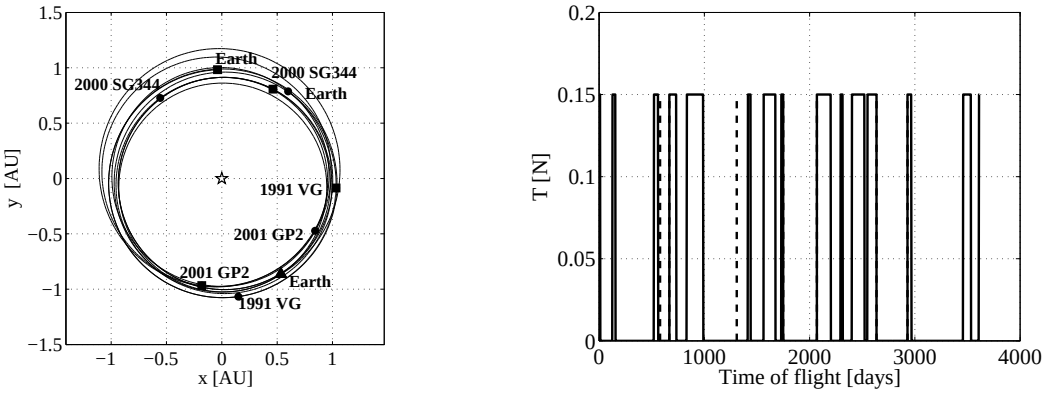

(a) Optimal trajectory (b) Thrust profile

Figure 7. 3^{rd} GTOC optimal solution.

generated by two primaries of masses m_1 and m_2, in motion about their center of mass. When primaries are assumed to move on circular orbits then a CRTBP is defined. A large literature is available on CRTBP, on the possibility of designing low-energy transfers within this dynamical framework, and the combination with low-thrust propulsion. The reader may refer to Mingotti et al. (2011), Ozimek and Howell (2010) and the references therein for more details. The following subsections show how the combination of indirect methods and parametric optimization can be exploited to design low-thrust and low-energy transfers in the CRTBP without making explicit use of invariant manifolds. The analysis is restricted to the Earth–Moon system.

5.1. *Equations of Motion*

The equations of motion can be conveniently expressed in a frame centered at the barycenter of the primaries and uniformly rotating with them. In this way, the primaries are fixed on the x-axis, the y-axis is in their plane of motion, and the z-axis completes the right-handed triad. By assuming a reference length equal to the distance between the two primaries, a reference mass equal to the sum of the primaries masses, and a reference time $1/\omega$ (where ω is the angular velocity of the secondary body with respect to the primary), the equations of motion are simplified (Szebehely 1967). These dimensionless equations can be presented in the first-order form of Eq. (1), where the expression of $\boldsymbol{g}$ can be written as the sum of two terms:

$$\boldsymbol{g_1}(\boldsymbol{r}) = \begin{bmatrix} x - (1-\mu)\dfrac{(x+\mu)}{r_1^3} - \mu\dfrac{(x-1+\mu)}{r_2^3} \\ y - \dfrac{(1-\mu)y}{r_1^3} - \mu\dfrac{y}{r_2^3} \\ -\dfrac{(1-\mu)z}{r_1^3} - \mu\dfrac{z}{r_2^3} \end{bmatrix} \tag{31}$$

where x, y and z are the components of the spacecraft position in the rotating frame,

whereas

$$r_1 = \sqrt{(x+\mu)^2 + y^2 + z^2} \tag{32}$$

$$r_2 = \sqrt{(x+\mu-1)^2 + y^2 + z^2}, \tag{33}$$

and a second term, given by

$$\boldsymbol{g_2}(\boldsymbol{v}) = \begin{bmatrix} 2v_y \\ -2v_x \\ 0 \end{bmatrix} \tag{34}$$

where v_x and v_y are the components of the spacecraft velocity in the rotating frame. Therefore, the ODE system depends on one parameter only, namely the mass parameter

$$\mu = \frac{m_2}{m_1 + m_2} \tag{35}$$

5.2. *Boundary Conditions*

Geocentric circular orbits, geosynchronous transfer orbits (GTO), and halo orbits are considered here as possible options for a departure. A halo orbit either around L_1 or L_2 is the only considered target orbit. In all cases the OCP is simplified by considering transfers between fixed states in an assigned time of flight. Similarly to the case of two-body transfers, the optimization of the initial state, final state, and transfer time is achieved by embedding the BVP into a parametric optimization problem. As a result, the initial and final boundary conditions become

$$\boldsymbol{\Psi}^0 \triangleq \begin{bmatrix} \boldsymbol{r}(t_0) - \boldsymbol{r}_0(\boldsymbol{\chi}^0) \\ \boldsymbol{v}(t_0) - \boldsymbol{v}_0(\boldsymbol{\chi}^0) \\ m(t_0) - m_0 \end{bmatrix} = 0 \tag{36}$$

and

$$\boldsymbol{\Psi}^f \triangleq \begin{bmatrix} \boldsymbol{r}(t_f) - \boldsymbol{r}_f(\boldsymbol{\chi}^1) \\ \boldsymbol{v}(t_f) - \boldsymbol{v}_f(\boldsymbol{\chi}^1) \end{bmatrix} = 0 \tag{37}$$

in which the dependence of both the initial and final states on the decision vector $\boldsymbol{\chi}$ is highlighted. Within the CRTBP no intermediate constraints are considered and then the solution of the OCP results in a BVP with only an initial (labelled with 0) and a final (labelled with either f or 1) node, i.e. a two-point BVP (TPBVP).

5.3. *Optimal Control Problem Formulation*

The Hamiltonian in the CRTBP is

$$\mathcal{H} = \boldsymbol{\lambda}_{\boldsymbol{r}}^T \boldsymbol{v} + \boldsymbol{\lambda}_{\boldsymbol{v}}^T \left(\boldsymbol{g_1}(\boldsymbol{r}) + \boldsymbol{g_2}(\boldsymbol{v}) + T_{max} \frac{u}{m} \boldsymbol{\alpha} \right) - \lambda_m \frac{T_{max}}{I_{sp} g_0} u + \frac{T_{max}}{I_{sp} g_0} u \tag{38}$$

As the functional dependence of the Hamiltonian on $\boldsymbol{\alpha}$ and u is the same as for the two-body problem it follows that also the optimal control solution is unchanged, i.e. is given by Eq. (12).

The costate differential equations in this case are

$$\dot{\boldsymbol{\lambda}}_{\boldsymbol{r}} = -\boldsymbol{G}_1(\boldsymbol{r})^T \boldsymbol{\lambda}_{\boldsymbol{v}} \tag{39}$$

$$\dot{\boldsymbol{\lambda}}_{\boldsymbol{v}} = -\boldsymbol{\lambda}_{\boldsymbol{r}} - \boldsymbol{G}_2(\boldsymbol{v})^T \boldsymbol{\lambda}_{\boldsymbol{v}} \tag{40}$$

$$\dot{\lambda}_m = -\frac{T_{max} u}{m^2} \lambda_v \tag{41}$$

where $\boldsymbol{G}_1(\boldsymbol{r})$ and $\boldsymbol{G}_2(\boldsymbol{v})$ are the gradients $\frac{\partial \boldsymbol{g}_1}{\partial \boldsymbol{r}}$ and $\frac{\partial \boldsymbol{g}_2}{\partial \boldsymbol{v}}$, respectively.

5.4. *Numerical Approach to the Optimal Control Problem*

Three main differences in the practical solution of the OCP arise when the CRTBP is considered. The first one is that the departure and arrival conditions are not linked to a celestial body anymore, and this affects the definition of the set of decision variables. In addition, when departing orbit has a low semi-major axis and the acceleration available from the propulsive system is small (as for current spacecraft with electric thrusters), the optimal solution includes long thrust arcs with many revolutions around the Earth (referred to as spiral arcs). This initial phase significantly complicates the numerical solution of the OCP. The last significant difference is that it is more difficult to generate first guesses for the fuel-OCP due to the higher nonlinearities of the dynamics; and the approach presented previously (energy problem followed by continuation) is not sufficiently robust in this case. The following subsections address these three points.

5.4.1. *Initial and Final Orbits*

In principle, the starting geocentric orbit can be optimized to reduce the mass consumption of the transfer. This means finding the optimal parameters of the parking orbit, compatible with the performance of the selected launcher. In practical cases the parking orbit is generally given and/or only a subset of orbital parameters can be considered as design variables. In this work only two options for the initial parking orbit are taken into account: a circular orbit of assigned altitude and a geosynchronous transfer orbit (GTO). In addition, the possibility of departing from these orbits with an impulsive kick Δv_0 is considered, in the view of possible future implementations of hybrid systems (Mingotti et al. 2013).

In case of a circular parking orbit the associated decision vector $\boldsymbol{\chi}^0 = [\chi_i^0; \chi_\Omega^0; \chi_\theta^0; \chi_{\Delta v}^0; \boldsymbol{\chi}_{\boldsymbol{u}_{\alpha,\delta}}^0]$, in which i, Ω, and θ are the parking orbit inclination, right ascension of ascending node, and true anomaly. The last two decision variables are used to include the initial impulsive maneuver option. For an initial GTO the decision vector is $\boldsymbol{\chi}^0 = [\chi_\omega^0; \chi_\theta^0; \chi_{\Delta v}^0; \boldsymbol{\chi}_{\boldsymbol{u}_{\alpha,\delta}}^{\boldsymbol{0}}]$, in which the ω is the angle between the x axis of the synodic and the apsidal line of the GTO. Finally, when the departure occurs from a halo orbit, the design vector reduces to $\chi^0 = \chi_{\tau_h}^0$, in which τ_h is a time variable in $[0, T_h]$, with T_h the period of the halo orbit. A value of τ_h univocally identifies the starting point on the assigned halo orbit. In this case no initial Δv_0 is considered. For all these options the variables associated to the TPBVP are $\boldsymbol{\xi}^{\boldsymbol{0}} = [\boldsymbol{\xi}_{\boldsymbol{\lambda}_r}^0; \boldsymbol{\xi}_{\boldsymbol{\lambda}_v}^0; \xi_{\lambda_m}^0]$.

As far as the final conditions are concerned, the final orbit is restricted to a L_1 or

L_2 halo orbit. The injection point on the halo is again optimized by introducing a time variable $\tau_h \in [0, T_h]$ in the decision vector. Each point on the halo is univocally identified by this variable. Also in this case the problem is reduced in Meyer form by including the final mass in the design vector, thus $\boldsymbol{\chi^1} = [\chi^1_{\tau_h}, \chi^1_m]$.

5.4.2. *Spiral Arcs*

As previously mentioned, when the energy level of the parking orbit is low the first portion of the transfer will aim at rapidly increasing the orbit energy. This first phase is typically characterized by the thrust vector aligned with the velocity vector, whereas in the second part of the transfer the thrust changes direction in order to meet the final state constraint. Thus, as proposed by Mingotti et al. (2011), the trajectory is subdivided in two phases: the first one, identified as initial spiral, is designed assuming the control at its maximum allowable level and aligned with the velocity vector in the synodic frame

$$\boldsymbol{\alpha}(t) = \frac{\boldsymbol{v}(t)}{v(t)} \tag{42}$$

whereas the second trajectory leg, comprised between the initial spiral orbit and the prescribed halo orbit, is optimized by the fuel-OCP.

For the first phase of the trajectory a particle swarm optimizer (PSO) (Armellin et al. 2007) is run with the objective of maximizing the orbital energy within a given time τ_{max}. The variables that are optimized by the PSO are the $\boldsymbol{\chi}^0$ introduced in Sec. 5.4.1, i.e. the geometrical configuration of the parking orbit and the initial Δv. Thus, as the optimal value for $\boldsymbol{\chi}^0$ is computed by the PSO, this vector is removed from the parametric optimization problem and substituted with a new design parameter τ_s. This is a time variable that univocally defines a point on the spiral orbit. This point is optimized by the parametric optimization by setting $\boldsymbol{\chi}^0 = \chi^0_{\tau_s}$.

5.4.3. *Solution Procedure*

To generate first guesses for the fuel-OCP the so-called ACT, developed by Ranieri and Ocampo (2005), is adopted. This approach consists substantially in a transformation, in the spacecraft velocity frame, to map initial costates into more physical parameters

$$(\boldsymbol{\lambda_{r}}_0, \boldsymbol{\lambda_{v}}_0) = \mathcal{T}(\beta, \dot{\beta}, \gamma, \dot{\gamma}, \lambda_{v0}, \dot{\lambda}_{v0}) \tag{43}$$

where β and γ are the in- and out-of-plane orientation angles of the thrust vector $\boldsymbol{u}$, respectively. Note, however, that the adjoint control transformation is only used to initialize the position and velocity costates, whereas the computation of costates at successive times is obtained by directly integrating Eq. (41).

Consequently, the optimization process in the case of geocentric parking orbit can be summarized as

(1) Run the global optimizer with the objective of maximizing the orbital energy in a given time, using the maximum thrust aligned with the velocity direction;
(2) Formulate the parametric optimization problem with decision vectors

$$\boldsymbol{\Xi} = [\xi^0_\beta; \xi^0_{\dot{\beta}}; \xi^0_\gamma; \xi^0_{\dot{\gamma}}; \xi^0_{\lambda_v}; \xi^0_{\dot{\lambda}_v}; \xi^0_{\lambda_m}] \tag{44}$$

$$\boldsymbol{\chi} = [\chi^0_{\tau_s}; \chi^1_{t_1}; \chi^1_{\tau_h}; \chi^1_m], \tag{45}$$

Table 5. Circular orbit to L_1 halo: search space and solution for the $\boldsymbol{\chi}$ subset of optimization variable

	Time of flight [days]	Ω_0 [rad]	i_0 [rad]	θ_0 [rad]	τ_h [TU]	m_f [$\%m_0$]
Upper Bound	50	2π	$\pi/2$	2π	T_h	1
Lower Bound	30	0	-$\pi/2$	0	0	0.5
solution	48.62	2.85	0.04	0.133	3.33	0.988

initial conditions

$$\boldsymbol{C}^0 \triangleq \begin{bmatrix} \boldsymbol{r}(t_0) = \boldsymbol{r}(\chi^0_{\tau_s}) \\ \boldsymbol{v}(t_0) = \boldsymbol{v}(\chi^0_{\tau_s}) \\ m(t_0) = m_0 \\ \boldsymbol{\lambda_r}(t_0) = \mathcal{T}_{\boldsymbol{\lambda_r}}(\xi^0_\beta, \xi^0_{\dot\beta}, \xi^0_\gamma, \xi^0_{\dot\gamma}, \xi^0_{\lambda_v}, \xi^0_{\dot\lambda_v}) \\ \boldsymbol{\lambda_v}(t_0) = \mathcal{T}_{\boldsymbol{\lambda_v}}(\xi^0_\beta, \xi^0_{\dot\beta}, \xi^0_\gamma, \xi^0_{\dot\gamma}, \xi^0_{\lambda_v}, \xi^0_{\dot\lambda_v}) \\ \lambda_m(t_0) = \xi^0_{\lambda_m} \end{bmatrix} \tag{46}$$

and final constraints

$$\boldsymbol{\Psi}^1 \triangleq \begin{bmatrix} \boldsymbol{r}(t_f^-) - \boldsymbol{r}(\chi^1_{\tau_h}) \\ \boldsymbol{v}(t_f^-) - \boldsymbol{v}(\chi^1_{\tau_h}) \\ m(t_f^-) - \chi^1_m \\ \lambda_m(t_f^-) \end{bmatrix} = 0 \tag{47}$$

(3) Solve the parametric optimization problem with control law given by Eq. (30), starting from $p = 1$, for increasing values of the continuation parameter;
(4) Solve the discontinuous problem with primer vector control law (12).

When the transfer starts from a halo orbit (or a highly energetic parking orbit) then the step 1 is not necessary. The decision variable $\chi^0_{\tau_s}$ is substituted by $\chi^0_{\tau_h}$, a time variable used to univocally determine the starting point on the initial orbit.

5.5. *Test Cases*

5.5.1. *Circular to L_1 Halo Transfer*

The first example is a transfer from an initial high circular orbit, with a radius $r_0 = 125000$ km, to an $A_z = 8000$ km halo orbit around L_1. The initial mass of the spacecraft is 1500 kg, while the maximum thrust assumed to be available is $T_{max} = 0.33$ N with an $I_{sp} = 3800$ s. Table 5 and 6 show the search space and the solution for all the optimization variables (TU stands for the time unit of the CRTBP). Note that in this particular case, in which the initial energy of the departure orbit is sufficiently high (i.e., no spiral arcs are necessary), the variables Ω_0, i_0, and θ_0 are included in the optimization vector $\boldsymbol{\chi}$.

Figure 8 presents the optimal trajectory in the synodic frame as well as the thrust profile. In this example the time of flight is approximately 49 days, and the final mass is

Table 6. Circular orbit to L_1 halo: search space and solution for the Ξ subset of optimization variable

	β_0	$\dot{\beta}_0$	γ_0	$\dot{\gamma}_0$	λ_{v_0}	$\dot{\lambda}_{v_0}$	λ_{m_0}
Upper Bound	2π	∞	$\pi/2$	∞	∞	∞	1
Lower Bound	0	-∞	-$\pi/2$	-∞	0	-∞	0
Solution	2.25	-0.0063	0.1224	-0.3656	0.0038	0.0529	0.02

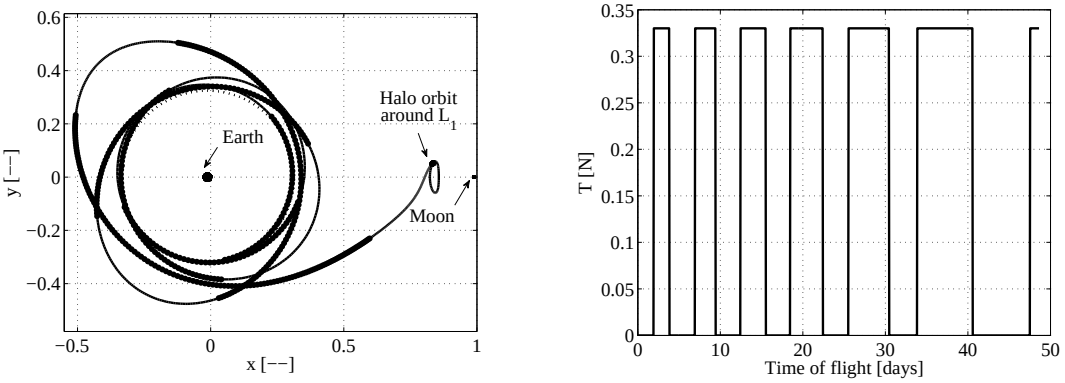

(a) Optimal transfer in synodic frame (b) Control low profile

Figure 8. Low-thrust transfer to a $A_z = 8000$ km L_1 halo orbit, departing from a $r_0 = 125000$ km circular orbit.

about 1481.5 kg with a propellant mass fraction of 1.233%. Note that the optimal control law has 13 switching points, and the optimal solution is computed without any need of including intermediate points.

5.5.2. *GTO to L_1 Halo Transfer*

The second example is a low-thrust transfer from an initial GTO orbit with perigee of 400 km to an $A_z = 8000$ km halo orbit around L_1. The spacecraft is characterized by an initial mass of 1000 kg, with a maximum thrust of 0.5 N and a $I_{sp} = 3000$ s as in Mingotti et al. (2011). As described in Sec. 5.4.2 the orientation of the GTO with respect to the Earth-Moon line (referred to as ω) is optimized through the PSO. The optmization has the goal of maximizing the orbital energy in a given time, in which the thrust is always active and aligned with the velocity vector. The search space for ω is $[0, 2\pi]$ rad, while the value of Δv_0 is set to zero. The optimal value obtained is $\omega = 0.078$ rad.

Tables 7 and 8 show the search space and the solution for all the optimization variables. The optimal transfer, in the synodic frame and the thrust profile are shown in Figure 9.

The obtained propellant mass fraction m_p/m_0 of 9.25% is very close to the best value of 9% reported in Mingotti et al. (2011), where the authors used a direct method to solve

Table 7. GTO to L_1 halo: search space and solution for the $\boldsymbol{\chi}$ subset of optimization variables

	Time of flight [days]	τ_s [TU]	τ_h [TU]	m_f [$\%m_0$]
Upper Bound	35	18.39	T_h	1
Lower Bound	10	0	0	0.5
solution	18.89	13.39	2.38	0.9074

Table 8. GTO to L_1 halo: search space and solution for the $\boldsymbol{\Xi}$ subset of optimization variables

	α_0	$\dot{\alpha}_0$	β_0	$\dot{\beta}_0$	λ_{v_0}	$\dot{\lambda}_{v_0}$	λ_{m_0}
Upper Bound	0.5	10	0.5	10	0.1	0.1	1
Lower Bound	-0.5	-10	-0.5	-10	0	-0.1	0
Solution	0.298	-0.875	-0.500	-0.024	0.032	0.020	1.1e-2

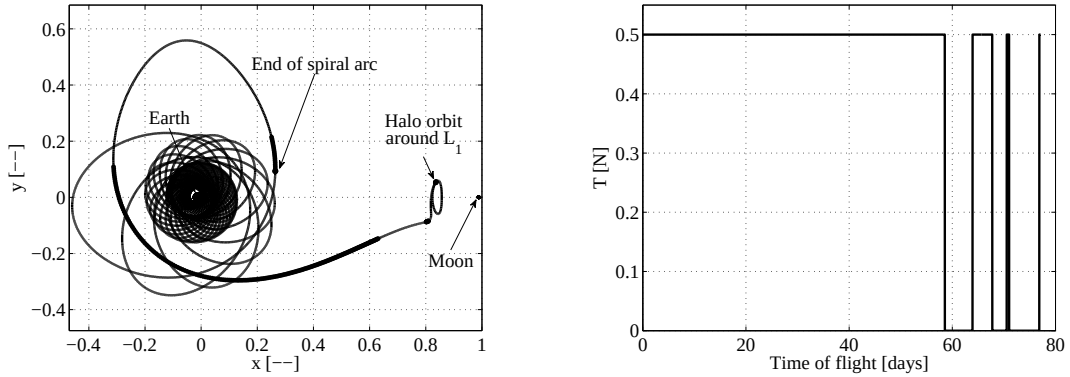

(a) Optimal transfer in synodic frame (b) Control low profile

Figure 9. Low-thrust transfer to the $A_z = 8000$ km L_1 halo orbit, departing from a GTO with a initial ω of 0.078 rad.

the optimal control problem and adopted the approach of targeting stable manifolds of the final Halo orbit rather then points on the orbit itself. On the other hand, note that the proposed solution reduces the transfer time from 91 to 77.11 days, and no information on invariant manifolds is used. In addition, the total number of optimization variables is only 10, which is 2–3 orders of magnitude less than with a direct method approach.

5.5.3. *L_1 Halo to L_2 Halo Transfers*

As last example, a transfer from an L_1 halo orbit to an L_2 halo orbit is shown. Both the halos have an amplitude $A_z = 8000$ km. The spacecraft initial mass is 1000 kg, with a maximum thrust of 0.5 N and $I_{sp} = 3000$. The optimal solution and search space boundaries are listed in Table 9 and 10.

Table 9. Halo to halo transfer: search space and solution for the $\boldsymbol{\chi}$ subset of optimization variable.

	Time of flight [days]	τ_{h1} [TU]	τ_{h2} [TU]	m_f [$\%m_0$]
Upper Bound	35	2.7459	3.4086	1
Lower Bound	5	0	0	0.5
Solution	13.48	0.3451	1.4874	0.9974

Table 10. Halo to halo transfer: search space and solution for the $\boldsymbol{\Xi}$ subset of optimization variable

	α_0	$\dot{\alpha}_0$	β_0	$\dot{\beta}_0$	λ_{v_0}	$\dot{\lambda}_{v_0}$	λ_{m_0}
Upper Bound	0.5	10	0.5	10	0.1	0.1	1
Lower Bound	-0.5	-10	-0.5	-10	0	-0.1	0
Solution	-0.4561	0.6337	0.3457	0.0836	0.0395	-0.0606	2.8e-3

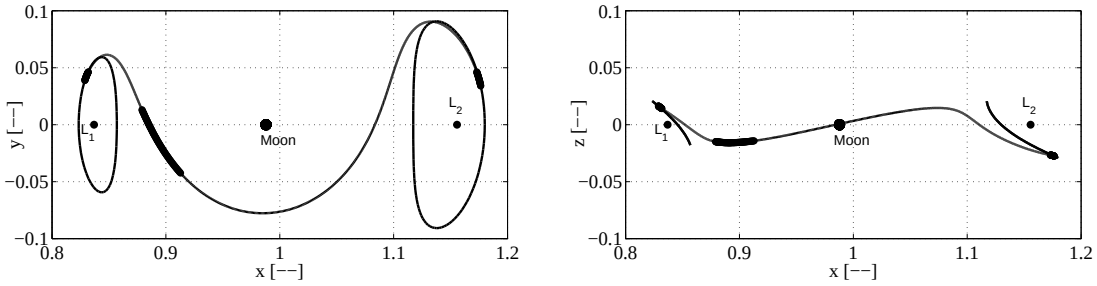

(a) Optimal transfer in synodic frame: x-y projection

(b) Optimal transfer in synodic frame: x-z projection

Figure 10. Low-thrust transfer from an $A_z = 8000$ km L_1 halo orbit to an $A_z = 8000$ km L_2 halo orbit.

In this case, the starting point is sought following the same strategy illustrated for the final point, thus there are two time variables, τ_{h1} and τ_{h2}, that univocally identify a point on the initial and final halo orbit respectively.

The corresponding trajectory is presented in Figure 10. The transfer starts with the engine on duty to leave the initial halo orbit. At the arrival, a small thrust arc is used to match the state on the final halo orbit in finite time. The fuel-optimal solution consists of a transfer of approximately 13.5 days with an overall propellant consumption of about 0.265%.

6. Conclusion

A method for the optimization of low-thrust transfers in the two-body and three-body dynamics was presented in this paper. The core of the approach is to formulate the optimization problem via an indirect method and to embed the resulting MPBVP in a parametric optimization. This facilitates the formulation of the trajectory optimization problem by using a limited number of variables and a reduced set of transversality conditions. A continuation approach based on a $\mathcal{C}^\infty$ representation of the "bang-bang" optimal control law is proposed. This is shown to be an effective technique to gain the convergence to the discontinuous fuel-optimal control law.

For the trajectory design in the two-body dynamics the first guess solutions were obtained with a low-fidelity tool for trajectory optimization. In addition, the energy-optimal control problem was solved before switching to the fuel-optimal one.

For the three-body dynamics case, first guesses solutions for the Lagrangian multipliers were obtained via the ACT. Spiral arcs were managed separately by using a global optimizer, whose goal was to maximize the orbital energy in a fixed amount of time using the maximum thrust aligned with the velocity.

A wide set of test cases was presented highlighting the effectiveness of the approach in dealing with complex transfers design even in the presence of high nonlinearties. In particular, for the CRTBP it was shown that a proper formulation of the control problem enables the computation of fuel-optimal transfer without the need of a prior knowledge about the solution.

Acknowledgment

The authors are grateful to Dr. Martín Lara for the careful reading of the manuscript.

References

Armellin, R., *et al.*, 2007. Aerogravity Assist Maneuvers: Coupled Trajectory and Vehicle Shape Optimization. *Journal of Spacecraft and Rockets*, 44(5), 1051–1059.

Bertrand, R., and Epenoy, R., 2002. New Smoothing Techniques for Solving Bang-Bang Optimal Control Problems-Numerical Results and Statistical Interpretation. *Optimal Control Applications and Methods*, 23(4), 171–197.

Betts, J.T, 1998. Survey of Numerical Methods for Trajectory Optimization. *Journal of Guidance, Control, and Dynamics*, 21(2), 193–207.

Bryson, A.E., and Ho, Y.C., 1969. *Applied Optimal Control: Optimization, Estimation, and Control*. Waltham: Blaisdell Publishing Company.

Bulirsch, R. and Stoer, J., 2002. *Introduction to Numerical Analysis*. Heidelberg: Springer.

Carrara, P., 2007. *Strategia per l'Ottimizzazione di Trasferimenti Spaziali*. MSc Thesis. Politecnico di Milano.

Casalino, L., Colasurdo, G., Sentinella M.R., 2007. Problem Description for the 3rd Global Trajectory Optimisation Competition. URL: `http://www.esa.int/gsp/ACT/doc/MAD/ACT-RPT-MAD-GTOC3-problem_stmt.pdf` [cited 20 May 2014]

Casalino, L., Colasurdo, G., Sentinella M.R., 2007. Results of

the 3rd Global Trajectory Optimisation Competition. URL: `mech.math.msu.su/~iliagri/gtoc3/resume.pdf` [cited 20 May 2014]

Conway, B., and Larson, K., 1998. Collocation Versus Differential Inclusion in Direct Optimization. *Journal of Guidance, Control, and Dynamics*, 21(5), 780–785.

Enright, P., and Conway, B.A., 1992. Discrete Approximations to Optimal Trajectories Using Direct Transcription and Nonlinear Programming. *Journal of Guidance, Control, and Dynamics*, 15(4), 994–1002.

Fortescue, P. and Swinerd, G. and Stark, J., 2011. *Spacecraft Systems Engineering*. New York: John Wiley and Sons, Inc.

Gao, Y., and Kluever, C. A., 2004. Low-Thrust Interplanetary Orbit Transfers Using Hybrid Trajectory Optimization Method with Multiple Shooting. *In: AIAA/AAS Astrodynamics Specialist Conference and Exhibit*, 16–19 Aug., 2004, Providence, RI. AIAA Paper 2004-5088.

Hargens, J., and Coverstone, V., 2002. Low-Thrust Interplanetary Mission Design Using Differential Inclusion. *In: AIAA/AAS Astrodynamics Specialist Conference and Exhibit*, Aug., 2002. AIAA Paper 2002-4730.

Hargraves, C.R. and Paris, S.W., 1987. Direct Trajectory Optimization Using Nonlinear Programming and Collocation. *Journal of Guidance, Control and Dynamics*, 10(4), 338–342.

Herman, A., and Conway, B., 1998. Optimal, Low-Thrust, Earth-Moon Orbit Transfer. *Journal of Guidance, Control, and Dynamics*, 21(1), 141–147.

Jain, S., and Tsiotras, P., 2008. Trajectory Optimization Using Multiresolution Techniques. *Journal of Guidance, Control, and Dynamics*, 31(5), 1424–1436.

Jiang, F., Baoyin, H., and Li, J., 2012. Practical Techniques for Low-Thrust Trajectory Optimization with Homotopic Approach. *Journal of Guidance, Control, and Dynamics*, 35(1), 245–258.

Kaplan, M.H., 1976. *Modern Spacecraft Dynamics and Control*. New York: John Wiley and Sons, Inc.

Kluever, C.A., and Pierson, B.L., 1995. Optimal Low-Thrust Three- Dimensional Earth-Moon Trajectories. *Journal of Guidance, Control, and Dynamics*, 18(4), 830–837.

Kuninaka, H., *et al.*, 2005. Asteroid Rendezvous of Hayabusa Explorer Using Microwave Discharge Ion Engines. *In: The 29th International Electric Propulsion Conference*, 31 Oct.– 4 Nov., 2005, Princeton, NJ. IEPC-2005-10.

La Mantia, M., and Casalino, L., 2006. Indirect Optimization of Low-Thrust Capture Trajectories. *Journal of Guidance, Control, and Dynamics*, 29(4), 1011–1014.

Lawden, D.F., 1963. *Optimal Trajectories for Space Navigation*. London: Butterworths.

Marec, J.P., 1979. *Optimal Space Trajectories*. Amsterdam: Elsevier.

Mengali, G., and Quarta, A.A., 2007. Trajectory Design with Hybrid Low-Thrust Propulsion System. *Journal of Guidance, Control, and Dynamics*, 30(2), 419–426.

Mingotti, G., Topputo, F., and Bernelli-Zazzera, F., 2011. Optimal Low-Thrust Invariant Manifold Trajectories via Attainable Sets. *Journal of Guidance, Control, and Dynamics*, 34(6), 1644–1655.

Mingotti G., Topputo F., Massari M., 2013. Hybrid Propulsion Transfers for Mars Science Missions. *In: 23rd AAS/AIAA Spaceflight Mechanics Meeting*, 10–14 Feb., 2013, Kauai, HI. AAS 13-385.

Olympio, J.T., 2011. Optimal Control Problem for Low-Thrust Multiple Asteroid Tour Missions. *Journal of Guidance, Control, and Dynamics*, 34(6), 1709–1719.

Ozimek, M.T., and Howell K.C., 2010. Low-Thrust Transfers in the Earth-Moon System, Including Applications to Libration Point Orbits. *Journal of Guidance, Control, and*

Dynamics, 33(2), 533–549.

Pontryagin, L.S., *et al.*, 1962. *The Mathematical Theory of Optimal Processes*. New York: Wiley-Interscience.

Ranieri C.L., and Ocampo, C.A., 2005. Optimization of Roundtrip, Time-Constrained, Finite Burn Trajectories via an Indirect Method. *Journal of Guidance, Control, and Dynamics*, 28(2), 306–314.

Rayman, M.D., *et al.*, 2000. Results from the Deep Space 1 Technology Validation Mission. *Acta Astronautica*, 47(2), 475–487.

Russel, C.T., *et al*, 2005. Dawn Mission and Operations. *In: International Astronomical Union Symposium on Asteroids, Comets, and Meteors*, 7–12 Aug. 2005, Rio de Janeiro, Brazil.

Russell, R.P., 2007. Primer Vector Theory Applied to Global Low-Thrust Trade Studies. *Journal of Guidance, Control, and Dynamics*, 30(2), 460–472.

Sauer Jr, C.G., 1973. Optimization of Multiple Target Electric Propulsion Trajectories. *AIAA Paper 73-205*, Jan. 1973.

Szebehely, V.G., 1967. *Theory of Orbits, the Restricted Problem of Three Bodies*. New York and London: Academic Press.

Vadali, S.R. and Nah, R.S., 2001. Fuel-Optimal, Low-Thrust, Three-Dimensional Earth-Mars Trajectories. *Journal of Guidance, Control and Dynamics*, 24(6), 1100–1107.